Vacuum 127 (2016) 82–87

Contents lists available at ScienceDirect

Vacuum

journal homepage: www.elsevier.com/locate/vacuum

Short communication

# Influence of pulsed bias frequency on the etching of magnetic tunneling junction materials

Kyung Chae Yang [a], Sung Woo Park [a], Min Hwan Jeon [b], Viet Phuong Pham [b], Du Yeong Lee [c], Tae Hun Shim [c], Jea Gun Park [c], Geun Young Yeom [a, b, *]

[a] School of Advanced Materials Science and Engineering, Sungkyunkwan University, Suwon, Gyeonggi 16419, Republic of Korea
[b] SKKU Advanced Institute of Nano Technology (SAINT), Sungkyunkwan University, Suwon, Gyeonggi 16419, Republic of Korea
[c] Department of Electronics Engineering, Hanyang University, Seoul 133-791, Republic of Korea

ARTICLE INFO

*Article history:*
Received 21 December 2015
Received in revised form
15 February 2016
Accepted 16 February 2016
Available online 3 March 2016

*Keywords:*
MTJ
Bias frequency
Etch
Pulse
MRAM

ABSTRACT

The effect of different bias frequencies during the etching of magnetic tunneling junction materials in an inductively coupled plasma with rf pulse biasing (50% duty percentage) on etch characteristics was investigated. The decrease of rf bias frequency from 13.56 MHz to 400 kHz while keeping the same average dc bias voltage at −300 V increased not only the etch rates of MTJ related materials but also the etch selectivities. We observe improved etch characteristics of CoFeB and CoPt, and also improved etch profiles of CoPt, CoFeB and MTJ (CoPt/MgO/CoFeB) masked with nanoscale W(100 nm)/Ti(20 nm)/Ru(5 nm) at lower bias frequencies. The observed improvements are attributed to the higher sputter yields due to the wider ion energy distribution (with increase high energy component) for the metal carbonyl related compounds formed during the etching of MTJ materials with $CO/NH_3$ etchant gas.


## 1. Introduction

As the critical size of a semiconductor device is decreased to a nanometer scale, the number of materials used for the device processing are increased and the requirements related to etch uniformity, etch selectivity, etch profile, and etch damage are becoming more stringent. Dry etching technique has become a principle key process enabling technologies for sub 20 nm [1–3].

Previously, to satisfy etch characteristics for new semiconductor devices, different etch tools such as capacitively coupled plasmas, inductively coupled plasmas, microwave plasmas, etc. have been applied because the process changes of the dry etching are mainly dependent on the characteristics of the plasma used in the process. However, as the device size decreases down to tens of nanometer scale, in addition to these techniques, other techniques are required to control the plasma parameters. One of the etch techniques investigated recently is the pulsing technique. Even though pulsing tends to decrease the etch rates due to the no power period during the pulse off time, pulse plasma has been investigated as one of the most promising techniques for precise anisotropic etching at the tens of a nanometer scale and is playing an important role in optimizing the plasma processing environment [4,5]. Especially, pulsed source and/or pulse-biased etching techniques have been used widely to control the plasma ionization or dissociation characteristics in order to remove charge related problems, control the energy of ions, and to improve the plasma uniformity [6–8].

In recent years, spin transfer torque magnetic random access memory (STT-MRAM) has been investigated and found to be one of the next generation's most promising nonvolatile semiconductor devices. Magnetic tunneling junction (MTJ) is used as the core element of STT-MRAM [9,10] but, one of the great challenges of MTJ is etching because MTJ materials are not easily etched due to the fact that the elements that from the MTJ do not form volatile etch products with conventional etch gases. In addition, the MTJ pattern sidewall can easily become damaged during the etching and a nonvolatile sidewall residue is formed especially for nanometer scale MTJ features [11–13]. In a previous study, for the etching of the MTJ materials for STT-MRAM, $CO/NH_3$ pulse plasma has also been applied and high etch selectivity of magnetic materials and less sidewall residue of magnetic multilayer structures have been realized with pulse-biased plasma etching by forming more volatile etch products [14]. Furthermore, pulse biasing has also been shown

* Corresponding author. School of Advanced Materials Science and Engineering, Sungkyunkwan University, Suwon, Gyeonggi 16419, Republic of Korea.
*E-mail address:* gyyeom@skku.edu (G.Y. Yeom).

http://dx.doi.org/10.1016/j.vacuum.2016.02.008
0042-207X/

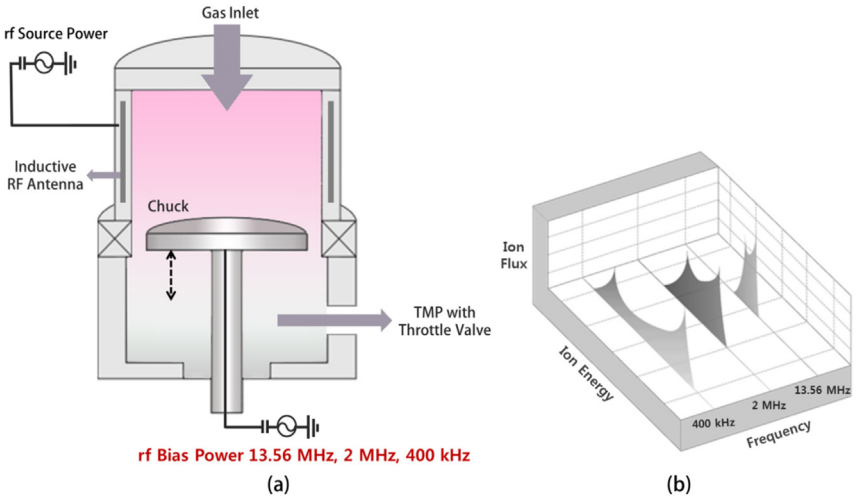


**Fig. 1.** (a) Schematic diagram of the rf bias pulsed ICP-type plasma etch system used in the experiment. (b) Cartoons showing the time averaged ion energy distribution for different rf bias frequencies while keeping the same average dc bias voltage to the substrate.

to control the etch profile of MTJ materials [15].

However, due to the difficulty in forming volatile etch products, the etching of magnetic materials for STT-MRAM devices is significantly dependent on the energy of the reactive ion bombarding the substrate during the etching. To achieve higher selectivity control and a vertical sidewall, the average energy of ions and ion energy distribution must be controlled [16,17]. One of the methods in increasing the energy of the ions for the same power to the substrate is to use a lower radio frequency (rf) power. In this work, the effect of rf pulse-biased inductively coupled plasma (ICP) etching process operated at 400 kHz–13.56 MHz, which can potentially have a significant effect on the control of the ion energy distribution with which ions bombard surfaces [18–20] and the etch characteristics of magnetic materials and transition metals are presented and discussed.

## 2. Experimental

The plasma etch system used in this experiment is a commercially available radio frequency inductively coupled plasma etch system (STS PLC) and the schematic diagram of the etch system is shown in Fig. 1(a). To form a high-density plasma, 500 W of continuous wave 13.56 MHz rf source power was supplied to one-turn copper coil located on the sidewall of the process chamber. For rf biasing the substrate, separate pulsed rf power generators with the frequencies of 400 kHz, 2 MHz, and 13.56 MHz were connected to the substrate to control the ion bombardment energy. The substrate bias power was pulsed at the pulse repetition frequency of 50 kHz and with a pulse duty percentage of 50% while keeping the substrate average dc bias voltage (that is, dc component of the sinusoidal voltage) at −300 V reading from the match box. In the case of the rf bias pulsing, it has found out that the etch selectivities appeared to be increased with the decrease of pulse duty ratio but the decrease of pulse duty ratio also decreases the etch rate. Therefore, in this study, we just fixed the pulse duty ratio at 50%. Fig. 1(b) shows the possible ion energy distribution to the substrate at different bias frequencies used in the experiment as suggested by previous researchers [21].

Blanket (non-patterned) thin films of MTJ layers such as CoPt, MgO, CoFeB, Co and W were prepared in addition to nanoscale patterned MTJ stack sample. Additionally some of the blanket samples were patterned with a photoresist material for etch rate and etch selectivity measurement. The MTJ stack was composed of CoPt (10 nm)/MgO (1 nm)/CoFeB (10 nm) on Ta (5 nm)/$SiO_2$ (25 nm)/silicon wafer. The MTJ stack, CoPt (20 nm) and CoFeB (20 nm) were masked with a patterned hardmask composed of W (100 nm)/Ti (20 nm)/Ru (5 nm). 50 sccm CO/$NH_3$ (1:3) was used as the reactive etch gas mixture. The operating pressure was kept at 6 mTorr for all experiments and the substrate temperature was kept at 80 °C.

The etch rate and etch selectivity were calculated by a surface profilometer (KLA Tencor Alpha-step 500) after measuring the sample etch depths. Also, the etch profiles of MTJ, CoFeB, and CoPt masked with the hardmsk were analyzed with field emission scanning electron microscopy (FE-SEM; Hitachi S-4700) and transmission electron microscopy (Cs-corrected TEM; Jeol JEM-ARM 200F) after the etching. Specimens for TEM were thinned to a final thickness of 100 nm by a low voltage (10 kV) focused ion beam (FIB; Jeol JIB-4601F) using a Ga ion beam. In addition, the chemical bonding states of the chemically reacted layer formed on the etched CoFeB surface were investigated by an X-ray photoelectron spectroscopy (XPS; VG Microtech ESCA2000) using Mg Kα radiation.

## 3. Results and discussion

Fig. 2(a) shows the etch rates of MTJ related materials such as CoPt, CoFeB, Co, MgO, and W (hardmask material). For CoFeB, two different compositions of Co:Fe:B (4:4:2) and Co:Fe:B (2:6:2) were used to investigate the effect of composition of CoFeB on the etch characteristics. The ICP source power of 500 W was fixed at continuous wave 13.56 MHz and the bias rf power frequency varied from 13.56 MHz to 400 kHz while maintaining the average dc bias voltage at −300 V with 50% duty percentage of the pulse bias power and 50 kHz of pulse frequency. As the process gas mixture, CO (12.5 sccm)/$NH_3$ (37.5 sccm) was used at 6 mTorr of operational pressure. As shown in Fig. 2(a), the decrease of substrate biasing frequency at the same average dc voltage generally increased the etch rates of MTJ related materials except for W and MgO. The etch rate of CoPt increased from 10.4 nm/min (13.56 MHz) to 14.9 nm/min (400 kHz) and that of Co increased from 6.7 nm/min (13.56 MHz) to 9.7 nm/min (400 kHz). In the case of CoFeB, even though the etch rate of

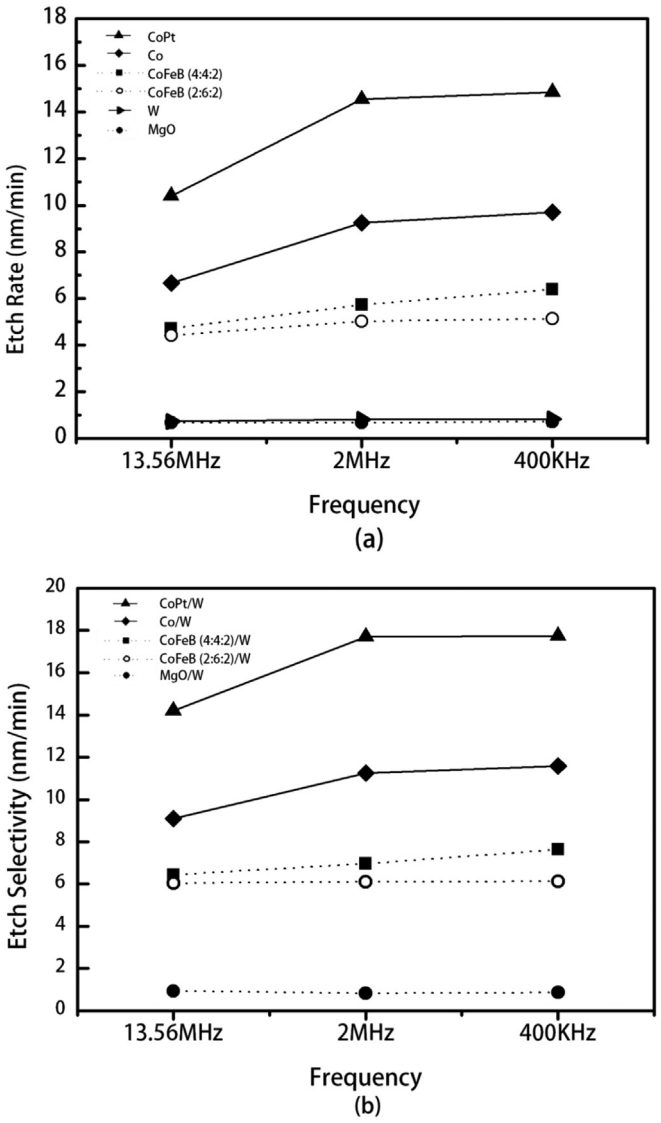


**Fig. 2.** (a) Etch rates of MTJ related materials such as CoPt, CoFeB (4:4:2 and 2:6:2), Co, MgO, and W (hardmask material) and (b) etch selectivities of CoFeB (4:4:2 and 2:6:2)/W, CoPt/W, Co/W, and MgO/W. As the ICP source power, 500 W of continuous wave 13.56 MHz was used and, as the bias power, −300 V of the average dc bias voltage was used while pulsing the bias power with the frequency of 50 kHz and duty percentage of 50%. The rf bias frequency varied from 13.56 MHz to 400 kHz. CO (12.5 sccm)/$NH_3$ (37.5 sccm) was used as the process gas mixture at 6 mTorr.

CoFeB (4:4:2) increased from 4.7 nm/min (13.56 MHz) to 6.4 nm/min (400 kHz), that of CoFeB (2:6:2) increased more slowly from 4.4 nm/min (13.56 MHz) to 5.1 nm/min (400 kHz). In the case of MgO and W, very slight increase or no significant increase of etch rate from 0.69 nm/min (13.56 MHz) to 0.73 nm/min (400 kHz) and from 0.73 nm/min (13.56 MHz) to 0.84 nm/min (400 kHz), respectively, was observed.

Fig. 2(b) shows the etch selectivitives of CoPt, CoFeB, Co, MgO over W for the conditions in Fig. 2(a). Due to the increase of etch rates of CoPt, CoFeB (4:4:2), Co with the decrease of bias frequency while showing no significant increase of etch rate of W, the etch selectivities of CoPt/W, CoFeB (4:4:2), and Co/W were increased by showing from 14.2 (13.56 MHz) to 17.7 (400 kHz), from 6.43 (13.56 MHz) to 7.6 (400 kHz), and from 9.1 nm/min (13.56 MHz) to 11.59 nm/min (400 kHz), respectively. On the contrary, the etch selectivities of CoFeB (2:6:2)/W and MgO/W did not change noticeably due to the similar change of etch rates with the decrease of bias frequency by showing from 6.04 nm/min (13.56 MHz) to 6.13 nm/min (400 kHz) and from 0.93 nm/min (13.56 MHz) to 0.87 nm/min (400 kHz), respectively.

The increased etch rates of MTJ related materials with the decrease of bias frequency are believed to be related to the increase of the width of the ion energy distribution of the lower bias frequency at the same average dc bias voltage as illustrated in Fig. 1(b). The increased width of ion energy distribution to the substrate with a decrease in rf frequency is well known and is related to the acceleration of the ions to the substrate by the instantaneous sheath voltage at the lower rf frequency while the ions bombarding the substrate at the higher frequency are accelerated by the average sheath voltage. Possibly due to the higher sputter yield of the etched MTJ materials at the higher ion bombardment energy, higher etch rates are believed to be obtained at the lower bias frequency.

In fact, during the etching with CO/$NH_3$, on the surface of the MTJ related materials, metal carbonyl related compounds can be formed. Metal carbonyls are formed on some of the materials such as Fe, Co, Pt, and W and no Mg carbonyls are known to be formed. In addition, the increase of etch selectivities of CoPt/W, CoFeB/W, and Co/W compared to MgO/W with the decrease of bias frequency is possibly related to the differences in the sputter yields of the metal carbonyl related compounds at different ion energies. Fig. 3 shows the XPS narrow scan data of Co and Fe of the CoFeB surfaces etched at different bias frequencies of 13.56 MHz ((a) and (b)) and 400 kHz ((c) and (d)). The CoFeB samples were etched using the conditions in Fig. 2 for 2 min. The peak binding energies of metallic Co and Fe were observed at 778.3 and 793.2 eV for Co 2*p*, and 707 and 720.2 eV for Fe 2*p*. In addition, on some of the samples, additional peaks possibly related to the metal oxide (or metal carbonyls) could be observed at 781 and 797.1 eV for Co, 710 and 723.5 eV for Fe. As shown in Fig. 3(a) and (b), in the case of Co, a broad Co-oxide related residue peak (or Co carbonyl related peak) was observed on the CoFeB surface before depth profiling for the bias frequency of 13.56 MHz. However, no such peak was observed on the CoFeB surface even before depth profiling for the bias frequency of 400 kHz. Higher peak intensities related to Fe-oxide residue (or Fe carbonyls) were observed for Fe XPS narrow scan data as shown in Fig. 3(c) and (d) and, similar to Co, a thicker Fe-oxide layer was remaining on the etched CoFeB surface for the bias frequency of 13.56 MHz compared to 400 kHz by showing the higher Fe-oxide related peak intensities during depth profiling. In the case of CoPt, possibly due to formation of more volatile carbonyls formed on the CoPt compared to CoFeB, no metal carbonyl (or metal oxide) peaks could be observed on the CoPt surfaces etched at different bias frequencies using XPS even before depth profiling (not shown).

The nanoscale masked MTJ stack composed of CoPt (10 nm)/MgO (1 nm)/CoFeB (10 nm), CoPt (20 nm), and CoFeB (20 nm) on Ta/$SiO_2$/Si wafer were etched for different bias frequencies and their etch profiles were observed by FE-SEM and the results are shown in Fig. 4. The MTJ stack, CoPt, and CoFeB were masked with a patterned 30 nm scale hardmask composed of W (100 nm)/Ti (20 nm)/Ru (5 nm). The etching was processed until the Ta layer on the silicon wafer was exposed. The etch conditions are the same as those in Fig. 2 and the etch time was adjusted to remove the MTJ related materials for three different materials. As shown in Fig. 4, all of the etched features showed more anisotropic etch profile at the lower bias frequency. As the bias frequency is decreased from 13.56 MHz to 400 kHz, the bottom sizes of the etched features decreased from 60 nm to 52 nm for CoFeB (4:4:2), from 59 nm to 51 nm for CoPt, and from 59 nm to 54 nm for MTJ. The improved

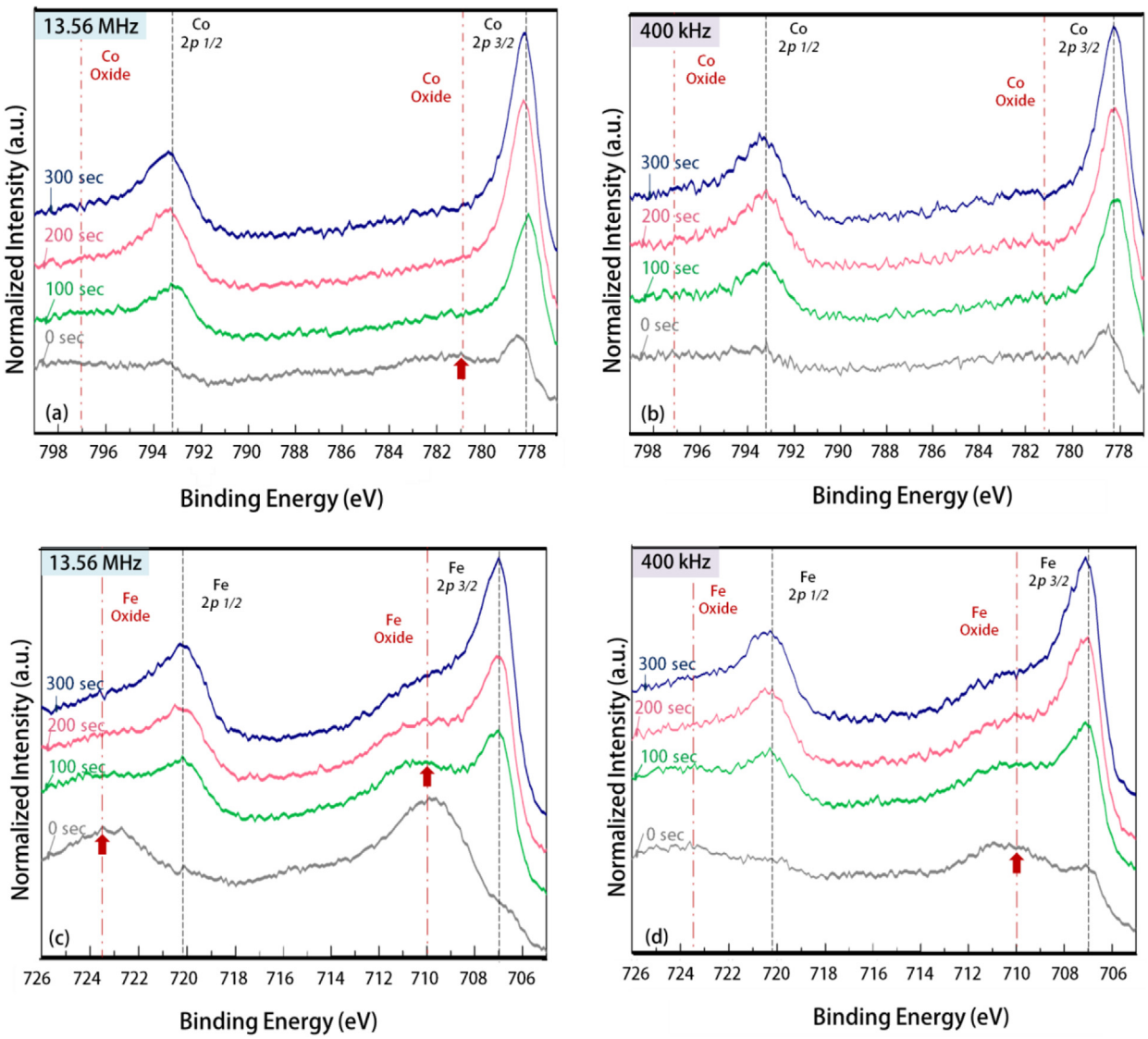


**Fig. 3.** XPS narrow scan data of (a) Co 2p and (b) Fe 2p of the CoFeB etched using the bias frequency of 13.56 MHz and (c) Co 2p and (d) Fe 2p of the CoFeB etched using the bias frequency of 400 kHz.

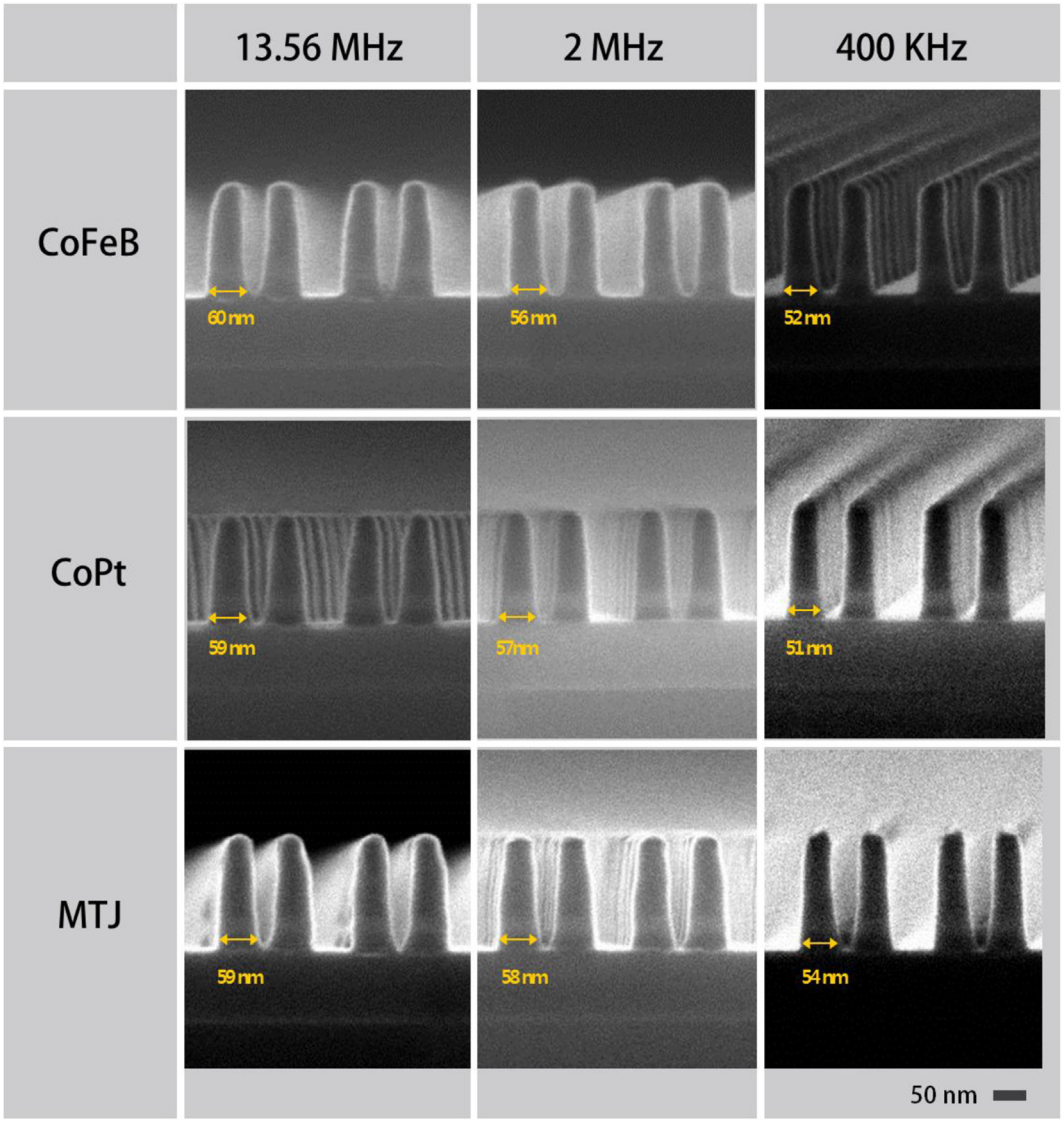


**Fig. 4.** SEM etch profile images of the nanoscale masked MTJ stack, CoPt (20 nm), and CoFeB (20 nm) on Ta/$SiO_2$/Si. The etch conditions are the same as those in Fig. 2 and the etching was processed until the Ta layer was exposed.

etch profiles observed at the lower bias frequency are believed to be partially related to improved etch selectivities of CoFeB/W and CoPt/W at the lower bias frequency observed in Fig. 2(b). The improved etch profiles at the lower bias frequency are also related to the thinner etch residue on the sidewall of the etched feature as shown in Fig. 3.

Using TEM, the CoFeB etch profiles observed for the bias frequencies of 13.56 MHz and 400 kHz were further observed and the results are shown in Fig. 5(a) for 13.56 MHz and (b) for 400 kHz. Cross-sectional TEM images were taken at the bottom of the features and, as shown in the images, the CoFeB etched with the bias frequency of 400 kHz showed the wider bottom gap between the CoFeB features compared to that etched with 13.56 MHz similar to the SEM images shown in Fig. 4.

## 4. Conclusions

The effect of the rf bias frequency on the etch characteristics of MTJ during the etching using $CO/NH_3$ ICP with rf bias pulsing was investigated. The decrease of rf bias frequency while keeping the same average dc bias voltage increased the etch rates of MTJ related materials such as Co, CoFeB (4:4:2), and CoPt while not significantly increasing the etch rates of and MgO and W. Therefore, the etch selectivities of CoPt/W, Co/W, and CoFeB (4:4:2)/W were improved with the decrease of the rf bias frequency even though no noticeable improvement of etch selectivites of MgO/W was observed. The improved etch selectivites of CoPt/W and CoFeB (4:4:2)/W at the lower rf bias frequency also improved etch profiles of MTJ stack for STT-MRAM in addition to the lower sidewall residue. The difference between the higher rf bias frequency and the lower rf bias frequency in the MTJ etching is the instant ion energy distribution. The observed improvement of the etch characteristics of MTJ materials at the lower rf bias frequency is believed to be related to the differences in the sputter yields at different ion energies of the metal carbonyl related compounds which are formed on the MTJ related materials during etching with $CO/NH_3$.

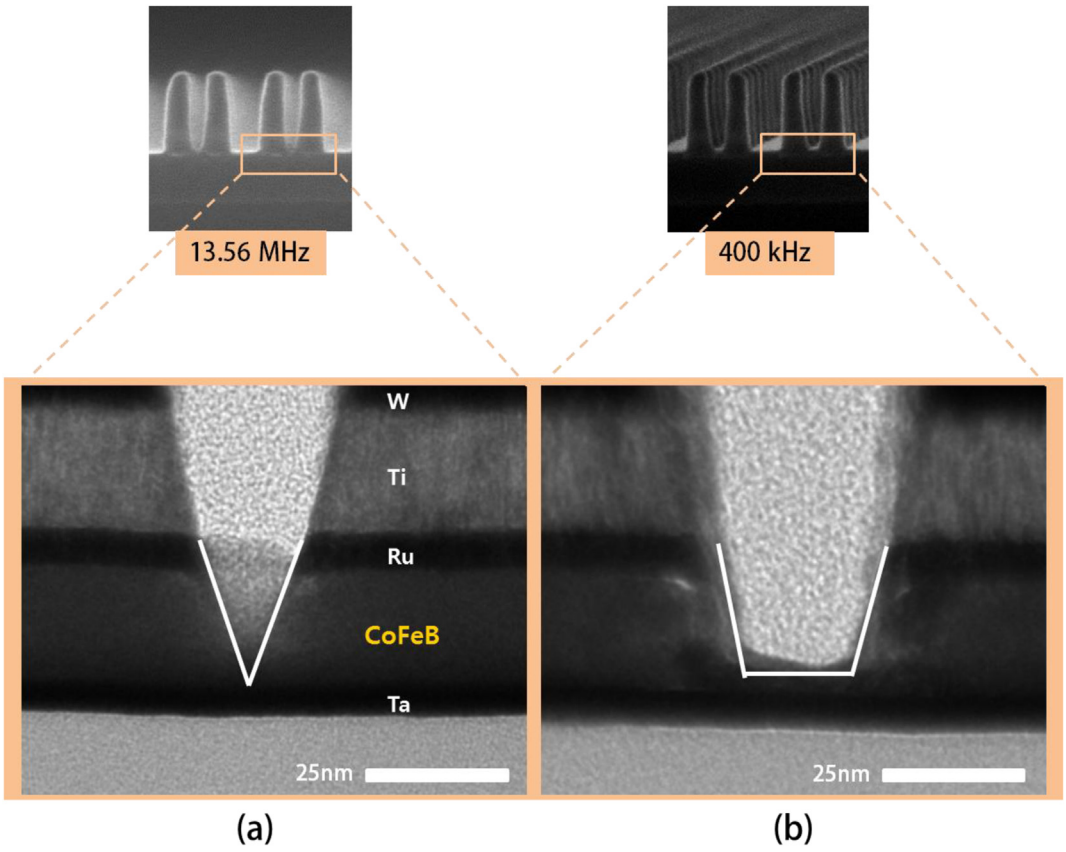


**Fig. 5.** Cross sectional TEM images of the bottom area between the CoFeB features etched using the bias frequency of (a) 13.56 MHz and (b) 400 kHz.

## Acknowledgements

The project was supported by the SRC project No. 2011-IN-2219 and Samsung Electronics. The authors would like to thank Dr. Satyarth Suri and Dr. Bob Turkot in Intel Corporation for helpful discussion on the MRAM etching.

## References

[1] J.K. Kim, S.I. Cho, S.H. Lee, C.K. Kim, K.S. Min, S.H. Kang, G.Y. Yeom, J. Vac. Sci. Technol. A 31 (2013) 0613101–0613107.
[2] X. Zhao, J.A. del Alamo, IEEE Electron. Device Lett. 35 (2014) 521–523.
[3] W. Kim, J. Jeong, Y. Kim, W.C. Lim, J.H. Kim, J.H. Park, H.J. Shin, Y.S. Park, K.S. Kim, S.H. Park, Y.J. Lee, K.W. Kim, H.J. Kwon, H.L. Park, H.S. Ahn, S.C. Oh, J.E. Lee, S.O. Park, S. Choi, H.K. Kang, C. Chung, IEDM Tech. Dig. (2011) 531–534.
[4] C.P. Etienne, M. Darnon, P. Bodart, M. Fouchier, G. Cunge, E. Pargon, L. Vallier, O. Joubert, S. Banna, J. Vac. Sci. Technol. B 31 (2013) 0112011–0112018.
[5] D. Borah, M.T. Shaw, S. Rasappa, R.A. Farrell, C. O'Mahony, C.M. Faulkner, M. Bosea, P. Gleeson, J.D. Holmes, M.A. Morris, J. Phys. D. Appl. Phys. 44 (2011) 174012.
[6] T. Mukai, H. Hada, S. Tahara, Hiroaki Yoda, S. Samukawa, Jpn. J. Appl. Phys. 45 (2006) 5542–5544.
[7] C.P. Etienne, M. Darnon, L. Vallier, E. Pargon, G. Cunge, F. Boulard, O. Joubert, S. Banna, T. Lill, J. Vac. Sci. Technol. B 28 (2010) 926–934.
[8] A. Agarwal, S. Rauf, Ken Collins, Appl. Phys. Lett. 99 (2011) 0215011–0215013.
[9] K. Kinoshita1, H. Honjo, S. Fukami, H. Sato, K. Mizunuma, K. Tokutome, M. Murahata1, S. Ikeda, S. Miura, N. Kasai, H. Ohno, Jpn. J. Appl. Phys. 53 (2014), 03DF031–03DF036.
[10] C.G.C.H.M. Fabrie, J.T. Kohlhepp, H.J.M. Swagten, B. Koopmans, M.S.P. Andriesse, E. van der Drift, J. Vac. Sci. Technol. B 24 (2006) 2627–2630.
[11] Y. Kim, S.C. Oh, W.C. Lim, J.H. Kim, W.J. Kim, J.H. Jeong, H.J. Shin, K.W. Kim, K.S. Kim, J.H. Park, S.H. Park, H. Kwon, K.H. Ah, J.E. Lee, S.O. Park, S. Choi, H.K. Kang, C. Chung, Symp. VLSI Technol. (2011) 210–211.
[12] J.H. Jeong, T. Endoh, Y. Kim, W.K. Kim, S.O. Park, J. Appl. Phys. 115 (2014), 17C7271–17C7273.
[13] L. Xue, L. Nistor, J. Ahn, J. Germain, C. Ching, M. Balseanu, C. Trinh, H. Chen, S. Hassan, M. Pakala, IEEE Trans. Magn. 50 (2014) 3401903.
[14] M.H. Jeon, H.J. Kim, K.C. Yang, S.K. Kang, K.N. Kim, G.Y. Yeom, Jpn. J. Appl. Phys. 52 (2013), 05EB031–05EB036.
[15] K.C. Yang, M.H. Jeon, G.Y. Yeom, Jpn. J. Appl. Phys. 54 (2015) 01AE011–01AE016.
[16] A. Agarwal, M.J. Kushner, J. Vac. Sci. Technol. A 23 (2005) 1440–1449.
[17] H. Shin, W. Zhu, L. Xu, V.M. Donnelly, D.J. Economou, Plasma Sources Sci. Technol. 20 (2011) 055001.
[18] R.J. Hoekstra, M.J. Kushner, J. Appl. Phys. 79 (1996) 2275–2286.
[19] W.M. Holber, J. Forster, J. Vac. Sci. Technol. A 8 (1990) 3720–3725.
[20] Daniel L. Flamm, J. Vac. Sci. Technol. A 4 (1986) 729–738.
[21] E. Kawamura, V. Vahedi, M.A. Lieberman, C.K. Birdsall, Plasma Source Sci. Technol. 80 (1999) R45–R64.